Energy Fuels **2010,** *24,* 5844–5850 · DOI:10.1021/ef100846r
Published on Web 11/03/2010

energy&fuels
article

Simulations of Axial Mixing of Liquids in a Long Horizontal Pipe for Industrial Applications

Lingling Zhao,[†,‡] Jos Derksen,[†] and Rajender Gupta*[,†]

[†]*Department of Chemical and Materials Engineering, University of Alberta, Edmonton, Alberta T6G 2G6, Canada, and* [‡]*School of Energy and Environment, Southeast University, Nanjing 210 096, People's Republic of China*

Received July 2, 2010. Revised Manuscript Received October 8, 2010

Various industrial applications require the use of common pipelines or tubing to simultaneously or sequentially deliver multiple types of liquids. Dependent upon the application, long pipelines or tubing can range from several meters to several kilometers in length, composed of significant horizontal and vertical sections. Axial mixing is an important aspect of such flows of liquids in succession from a safety and reliability point of view. It is anticipated that mixing is due to turbulence and buoyancy, with the latter as a result of density differences of the mixing fluids. This paper sets out a numerical simulation model based on computational fluid dynamics (CFD) to fundamentally understand the mixing behavior of two miscible fluids under actual industrial-project-specific conditions. To benchmark its accuracy, the simulation model is first verified with respect to its numerical parameters using a short, 10 m pipe. Subsequently, a 100 m horizontal pipe is modeled, and we show that these results can be used to extrapolate longer length pipes. Finally, the sensitivity of mixing with respect to the Reynolds and Richardson numbers (characterizing buoyancy) has been investigated.

1. Introduction

A number of fluids have been transported in succession in the same pipeline in the oil industry. These pipelines are large and use buffer fluids or solid pads to separate these fluids. However, in some cases, these methods may not be adopted.

Industrial burner/ignitor systems,[1,2] oil/fluid pipelines,[3,4] *in situ* oil recovery,[5,6] and underground coal gasification (UCG)[7,8] are just a few of the potential industrial applications where common pipelines or tubes are used for controlled delivery of a number of fluids, sometimes miscible and sometimes immiscible. An example of such an application is the UCG trials that occurred at El-Tremedal, Spain, and Washington, U.S.A., during the 1980s and 1990s.[9,10] Pyrophoric fluids were used to ignite UCG systems, such as in El Tremedal.[11] A silane/propane igniter and burner system was used for the first time in UCG experiments in the Tono Basin of Washington in the winter of 1981−1982. With this system, a small-diameter tube ($^1/_2$ in.) is inserted in the hole to the point where ignition is desired. The tube is then purged with nitrogen to drive out the air, and a charge of the pyrophoric gas silane (SiH_4) is forced through it. When the silane reaches the end of the tube, it bursts into flame upon exposure to the air. Finally, a fuel gas, such as methanol, is sent through the tube behind the silane to sustain the burn for as long as desired. The system was designed for both igniting coal and burning through a steel pipe from the inside to provide a new outlet from the pipe. In such cases, these fluids need to be transported through smaller pipelines. It becomes very critical to assess mixing of different fluids during their transportation.

The challenge is that there are potentially long distances between the injection point and delivery point and that the only place to control the process is from the injection point. Given the length of tubing, fluids may not arrive at the delivery point at the moment required. Also, fluids A and B flow down the same tubing, stringing one behind the other, whether any mixing might occur and, more generally, whether mixing is desirable or a problem.

With the above applications in mind, the present paper aims at estimating mixing in the axial (i.e., streamwise) direction between two initially separated miscible liquids flowing one after the other down a long horizontal pipe line. The conditions are such that we anticipate mildly turbulent flow (the Reynolds number based on the pipeline diameter and superficial velocity is of the order of 10^4−10^5). Therefore, turbulence is a source of mixing between the two liquids. For this analysis, the density difference between fluids A and B is 127 kg/m^3, so that (given the long horizontal stretch of the pipe line) buoyancy may contribute to mixing. Because fluid A

*To whom correspondence should be addressed. Telephone: +1-780-492-6861. E-mail: rajender.gupta@ualberta.ca.

(1) Millen, M. J.; Sowerby, B. D.; Coghill, P. J.; Tickner, J. R.; Kingsley, R.; Grima, C. *Flow Meas. Instrum.* **2000**, *11*, 153–158.
(2) Schlüter, J. U.; Schönfeld, T. *Flow, Turbul. Combust.* **2000**, *65*, 177–203.
(3) Langevin, D.; Poteau, S.; Hénaut, I.; Argillier, J. F. *Oil Gas Sci. Technol.* **2004**, *59*, 511–521.
(4) Zhang, Z. X.; Wang, G. X.; Massarotto, P.; Rudolph, V. *Energy Convers. Manage.* **2006**, *47*, 702–715.
(5) Duncan, I. J.; Nicot, J. P.; Choi, J. W. *Energy Procedia* **2009**, *1*, 2037–2042.
(6) Hasan, S. W.; Ghannam, M. T.; Esmail, N. *Fuel* **2010**, *89*, 1095–1100.
(7) Khadse, A.; Qayyumi, M.; Mahajani, S.; Aghalayam, P. *Energy* **2007**, *32*, 2061–2071.
(8) Blinderman, M. S.; Saulov, D. N.; Klimenko, A. Y. *J. Energy Inst.* **2008**, *81*, 7–13.
(9) Pirard, J. P.; Brasseur, A.; Coëme, A.; Mostade, M.; Pirlot, P. *Fuel* **2000**, *79*, 471–478.
(10) Brasseur, A.; Antenucci, D.; Bouquegneau, J. M.; Coëme, A.; Dauby, P.; Létolle, R.; Mostade, M.; Pirlot, P.; Pirard, J. P. *Fuel* **2002**, *81*, 109–117.
(11) Creedy, D. P.; Garner, K.; Holloway, S.; Jones, N.; Ren, T. X. Review of underground coal gasification technological advances. *Report Coal R211, DTI/Pub URN 01/1041*; Energy Technology Support Unit (ETSU), Department of Trade and Industry: London, U.K., 2001.

comes first and is heavier than fluid B, buoyancy-driven mixing in the vertical portion is not an issue in this situation. Potentially extreme pressure conditions also need to be considered. For this analysis, the fluid A and fluid B mixture is at pressures in the range of 5−20 MPa, which would make experimentation a harsh exercise. We develop our understandings of the behavior of the fluids via numerical simulation; i.e., we simulate the turbulent flow including the mixing in the pipeline by means of computational fluid dynamics (CFD). The potential contribution of buoyancy to axial mixing (in addition to turbulence) and the different viscosities of the fluids involved are the main reasons that we revert to CFD and cannot base our estimates on single-component correlations for axial dispersion coefficients developed in seminal works, e.g., Taylor[12] and Tichacek et al.,[13] and later extended by many other researchers, e.g., ref 14.

This paper is organized in the following manner: First, we describe the numerical model and examine it with different parameters using a 10 m pipe. This allows us to efficiently select the appropriate numerical parameters, such as grid spacing and (because we perform transient simulations) time step. Then, we present modeling results for a 100 m length leg and estimate fluid A and fluid B mixture lengths in the axial direction. Subsequently, the 100 m results are extrapolated to several kilometer lengths, and we draw conclusions relevant to the specific industrial process that interests us. Finally, we comment on the sensitivity of our results with respect to the Reynolds number and density ratio.

2. Numerical Models and Methods

The time-dependent convection−diffusion equation for a scalar α with concentration Y_α is as follows:

$$\frac{\partial Y_\alpha}{\partial t} + u_i \frac{\partial Y_\alpha}{\partial x_i} = \frac{\partial}{\partial x_i}\left(D \frac{\partial Y_\alpha}{\partial x_i}\right) \tag{1}$$

(summation over repeated indices implied), where t is the time and D is the diffusion coefficient, which, in the case of turbulent flow, includes molecular and turbulent contributions.

The Navier−Stokes equation for incompressible flow reads

$$\frac{\partial u_i}{\partial t} + u_j \frac{\partial u_i}{\partial x_j} = -\frac{1}{\rho}\frac{\partial p}{\partial x_i} + \frac{\partial}{\partial x_j}\left(\nu \frac{\partial u_i}{\partial x_j}\right) \tag{2}$$

where ρ is the fluid density and ν is the viscosity. As for the scalar transport equation, in the case of turbulent flow, the viscosity includes molecular and turbulent contributions.

In liquid mixtures, the concentration diffusion flux can be described as follows:

$$J_{\alpha,i} = -\rho\left(D_\alpha + \frac{\nu_t}{Sc_t}\right)\frac{\partial Y_\alpha}{\partial x_i} \tag{3}$$

where $J_{\alpha,i}$ is the diffusion flux of species α (with concentration Y_α) in the ith coordinate direction, which arises because of a concentration gradient, D_α is the molecular diffusion coefficient of α, and Sc_t is the turbulent Schmidt number, $Sc_t = \nu_t/D_t$, where ν_t is the turbulent viscosity and D_t is the turbulent diffusivity. In the simulations presented here, we set $Sc_t = 0.7$, which is an often used value. It reflects the fact that the scalar spectrum extends to higher frequencies than the dynamic spectrum, so that scalar eddy diffusion is stronger than momentum eddy diffusion.[15] Note that turbulent diffusion generally overwhelms laminar diffusion and that the specification of detailed laminar diffusion properties in turbulent flows is generally not warranted.[16] As a result, eq 3 can be written as

$$J_{\alpha,i} = -\rho\frac{\nu_t}{Sc_t}\frac{\partial Y_\alpha}{\partial x_i} \tag{4}$$

The turbulent viscosity ν_t follows from the turbulence model. According to the standard $k-\varepsilon$ model that we use here, the turbulent viscosity ν_t is computed by combining the turbulent kinetic energy k and the rate with which it is dissipated (ε) as follows:

$$\nu_t = C_\mu \frac{k^2}{\varepsilon} \tag{5}$$

where C_μ is a constant. In the $k-\varepsilon$ model, next to solving the Navier−Stokes equation, we also solve equations for k and ε. The latter equations contain a number of unclosed terms that we model via semi-empirical relations that contain a set of parameters[17] that we give the following (default) values:

$$C_{1\varepsilon} = 1.44,\ C_{2\varepsilon} = 1.92,\ C_\mu = 0.09,$$
$$\sigma_k = 1.0,\ \text{and}\ \sigma_\varepsilon = 1.3$$

Another important phenomenon that should be considered is the effect of buoyancy. When a non-zero gravity field and a density gradient are present simultaneously, the standard $k-\varepsilon$ model accounts for the generation of k because of buoyancy by means of a source term G_b and a corresponding contribution to the production of ε. The generation of turbulence because of buoyancy is given by

$$G_b = g_i \frac{\nu_t}{Sc_t}\frac{\partial \rho}{\partial x_i} \tag{6}$$

where g_i is the component of the gravitational acceleration in the ith direction.

It is known that turbulent kinetic energy k tends to be augmented in unstable stratification;[18] the effect on ε is less clear. In the present simulations, the buoyancy effects on ε are neglected simply by setting G_b to 0 in the transport equation for ε. This implies that we may overestimate the effects of buoyancy on axial mixing and (because, in this specific application, axial mixing is generally unwanted) consider a worst-case scenario in this respect.

Finally, from penetration theory,[19] it follows that the mixing length of different species is dependent upon both turbulent diffusivity D_t and contact time t.

$$\delta = \sqrt{\pi t D_t} \tag{7}$$

This equation (essentially its $t^{1/2}$ behavior) will be used to extrapolate the results obtained for a 100 m long horizontal pipe to pipes with lengths of 1−3 km.

The flow solver used throughout this work is the CFD software Fluent, version 6.3.

3. Model Verification

In the simulations, we start by determining the fully developed turbulent flow of the fluid initially filling the pipe. This is

(12) Taylor, G. I. *Proc. R. Soc. London, Ser. A* **1956**, *223*, 446–468.
(13) Tichacek, L. J.; Barkelew, C. H.; Baron, T. *AIChE J.* **1957**, *3*, 439–442.
(14) Ekambara, K.; Joshi, J. B. *Chem. Eng. Sci.* **2003**, *58*, 2715–2724.
(15) Hartmann, H.; Derksen, J. J.; van den Akker, H. E. A. *AIChE J.* **2006**, *52*, 3696–3706.
(16) Perkins, G.; Sahajwalla, V. *Chem. Eng. Res. Des.* **2007**, *85*, 329–343.
(17) Wilcox, D. C. *Turbulence Modeling for CFD*, 1st ed.; DCW Industries: La Cañada, CA, 1993.
(18) Chandra, L.; Grötzbach, G. *Int. J. Heat Fluid Flow* **2008**, *29*, 743–751.
(19) van Elk, E. P.; Knaap, M. C.; Versteeg, G. F. *Chem. Eng. Res. Des.* **2007**, *85*, 516–524.

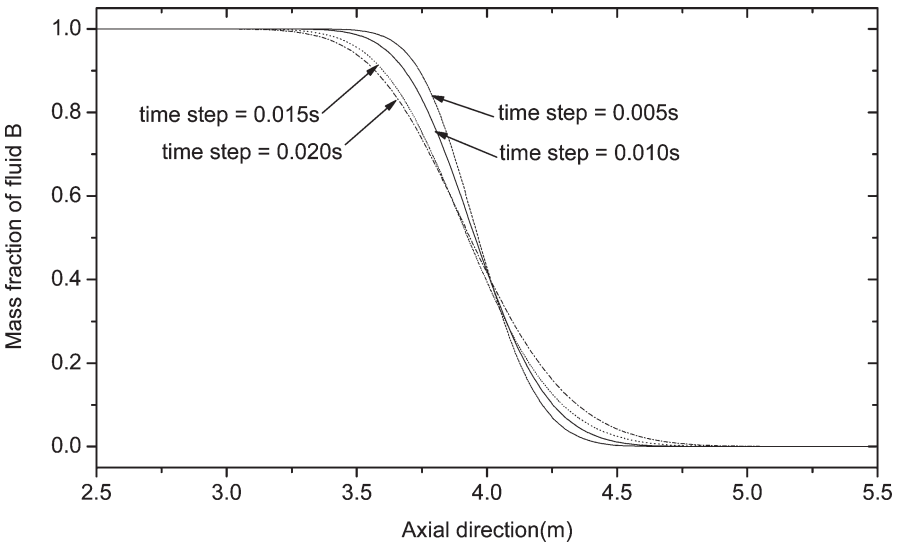

Figure 1. Mass fraction distribution of fluid B after 4 s using different time step sizes (grid size is 2 mm).

a steady-state simulation. Subsequently (at time equal to 0), we switch to an unsteady mode when we start feeding the second fluid. If the second fluid has the same viscosity and density as the first fluid (no buoyancy), the unsteady simulations only need to solve the scalar transport equation (eq 1). If buoyancy plays a role, the unsteady part of the simulations also alters the flow dynamics.

The diameter of the 3 km leg is 12 mm, i.e., a very long and slim pipe. Even for a two-dimensional model, a fine mesh and small time steps could make this system prohibitively computationally expensive. Therefore, we first modeled a 10 m leg to analyze the validity of our approach and to determine numerical parameters leading to acceptable accuracy and feasible computational expense. Then, we used this model and its parameters to solve the 100 m leg problem. From the results, we can deduce (on the basis of eq 7) the axial mixing in 1 and 3 km legs.

The densities of fluids A and B are 750 and 523 kg/m^3, respectively. Their viscosities are 0.3×10^{-3} and 0.048×10^{-3} kg m^{-1} s^{-1}. The initial Reynolds number of this system based on the superficial velocity in the pipe, u (= 1 m/s), its diameter, d (= 12 mm), is 30 000 with fluid A and then increases to 130 000 with fluid B. Buoyancy effects can be characterized by means of a second dimensionless number, e.g., the Richardson number, defined as $Ri = (gd\Delta\rho)/(v^2\rho)$. Under the standard conditions, it has a value of $Ri = 22 \times 10^{10}$.

Because the geometry is relatively simple, we use a structured mesh with a grid size of 20 in the transverse direction. At the wall, wall functions have been applied. The first grid point from the wall has a dimensionless distance to the wall of $y^+ = 20$ at the fluid B side and $y^+ = 27$ at the fluid A side. These y^+ values are within the validity range of the wall functions that have been applied. At the inlet, a uniform velocity, u, is imposed. At the outlet, there are no axial variation conditions. The grid size in the axial direction as well as the time step size in the transient parts of the simulations have been varied to assess their impact on the final results.

3.1. Effect of the Time Step Size. The time step size is an important factor in the unsteady-state model. For example, it relates to computation time and numerical diffusion. With an axial grid length of 2 mm and a 10 m long pipe, fluid B volume fraction profiles along the centerline 4 s after the start of injection of fluid B are shown in Figure 1 for different time step sizes (Δt = 0.005, 0.01, 0.0015, and 0.02 s). The diffusion between fluids A and B is obvious from Figure 1. As a measure for the level of mixing, we use the mixture length that is defined as the distance between the points that

Table 1. Numerical Modeling Case Data Summary Showing the Locations from the Inlet Where Mass Fractions of fluid A Are 0.9 and 0.1, Respectively

case number	grid length (mm)	time step (s)	0.9 point (m)	0.1 point (m)	mixture length (m)
1	1	0.01	3.68	4.25	0.57
2	1	0.02	3.59	4.33	0.74
3	1	0.03	3.51	4.42	0.91
4	2	0.005	3.74	4.21	0.47
5	2	0.01	3.68	4.28	0.60
6	2	0.015	3.63	4.32	0.69
7	2	0.02	3.58	4.33	0.75
8	2	0.03	3.5	4.43	0.93
9	4	0.01	3.74	4.39	0.65
10	4	0.02	3.55	4.36	0.81
11	4	0.03	3.5	4.45	0.95

case number	gravitational acceleration (m/s^2)	temperature (K) fluid B/A	0.9 point (m)	0.1 point (m)	mixture length (m)
5	9.8	300/300	3.68	4.28	0.60
12	9.8	350/300	3.66	4.25	0.60
13	9.8	350/300	3.61	4.28	0.67

case number	diameter (mm)	density ratio fluid B/A	0.9 point (m)	0.1 point (m)	mixture length (m)
14	12	0.1	3.46	3.99	0.53
15	12	0.3	3.58	4.14	0.56
16	12	0.5	3.64	4.22	0.58
5	12	0.7	3.68	4.28	0.60

case number	diameter (mm)	velocity (m/s)	0.9 point (m)	0.1 point (m)	mixture length (m)
17	6	2	7.39	8.46	1.07
5	12	1	3.68	4.28	0.60
18	24	0.5	1.7	2.21	0.51

case number	*Re* number	velocity (m/s)	0.9 point (m)	0.1 point (m)	mixture length (m)
19	10000	0.5	1.82	2.15	0.33
5	20000	1	3.68	4.28	0.60
20	40000	2	7.38	8.50	1.12

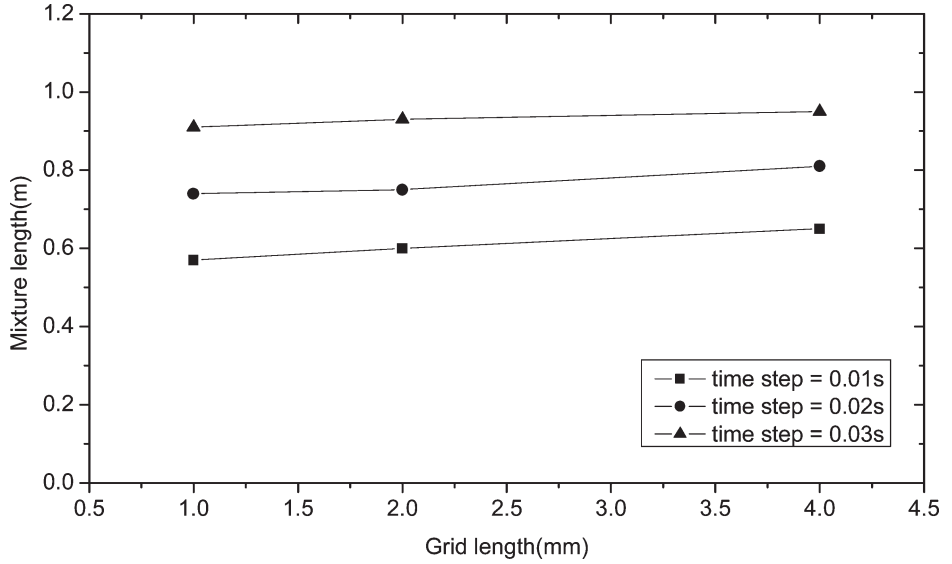

Figure 2. Effect of the grid size and time step on the mixture length after 4 s.

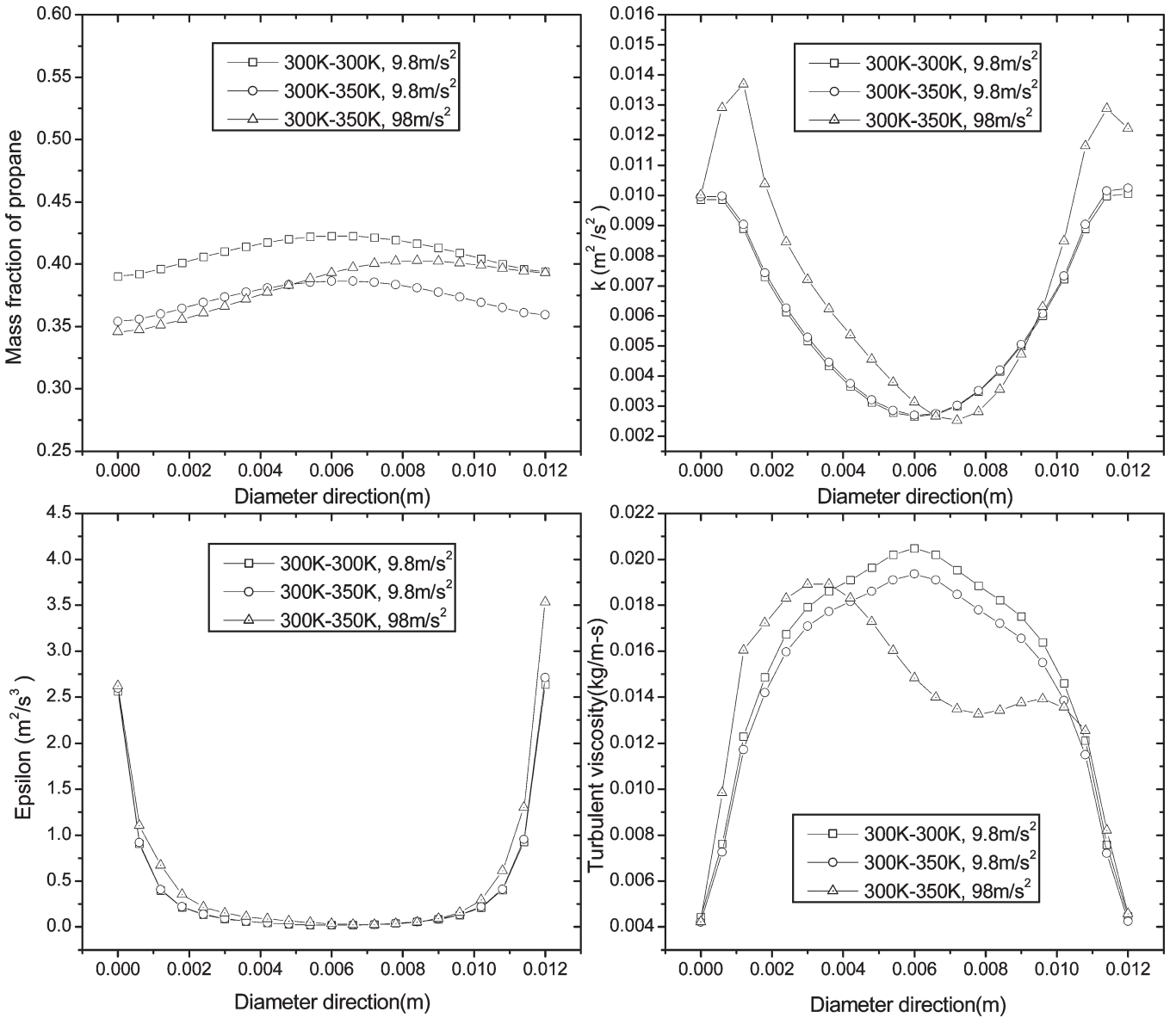

Figure 3. Mass fraction and turbulent parameters at a distance of 4 m from the inlet; effect of buoyancy.

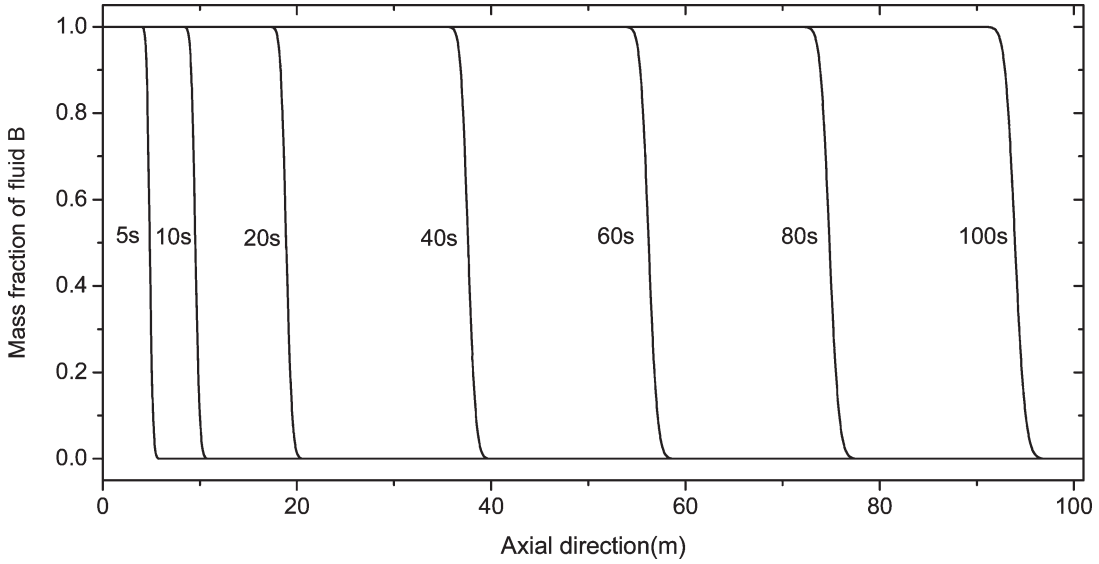

Figure 4. Mass fraction of fluid B in a 100 m horizontal pipe.

have fluid B volume fractions of 0.9 and 0.1. From the results in Figure 1, we can see that the mixture length depends upon the time step size. In Table 1, the values for the mixture length are given. Increasing the time step size gives rise to increased mixture lengths. The mixture length after only 4 s of contact time increases 25% if Δt is increased from 0.01 to 0.02 s. On the basis of the results in Figure 1 and Table 1, we chose $\Delta t = 0.01$ s as a compromise between accuracy and computational feasibility.

3.2. Effect of the Grid Size in the Axial Direction. Another important factor in terms of accuracy and computational workload is the grid size, specifically the grid size in the axial direction. For comparison, we calculated the mixing process with axial grid lengths of $\Delta x = 1$, 2, and 4 mm and $\Delta t = 0.01$, 0.02, and 0.03 s, respectively, while not altering the grid in the radial direction. The results 4 s after fluid B was injected are included in Table 1 and shown in Figure 2.

An increase in the grid size slightly enlarges the mixture length for any time step size. In fact, the slopes in Figure 2 are independent of Δt. On average, the mixture length difference between grids of 1 and 2 mm is 0.024 m, which is only a very small fraction of the mixture length; it is a much smaller effect than the time step size effect. On the basis of these results, the axial grid length is set to $\Delta x = 2$ mm throughout the rest of the simulations.

3.3. Effect of Buoyancy. As indicated above, buoyancy as a result of the density difference between fluids A and B may add to axial mixing. In Table 1, we show results in terms of the axial mixture length for three values of the Richardson number with the numerical parameters (time step and grid spacing) that we decided upon above. Because buoyancy induces asymmetry, we show profiles of the volume fraction of fluid B and various turbulence quantities across the pipe (Figure 3). It can be seen that there is not much difference between simulation results without buoyancy in the models ($Ri = 0$) and the results with $Ri = 22 \times 10^{10}$; the mixture length is hardly affected (Table 1), and profiles stay largely symmetric (Figure 3). Only if we increase Ri to 22×10^{11}, we see enhanced mixing in terms of an increase of the mixture length by some 10% and clearly asymmetric profiles.

4. Results and Analysis

4.1. Pipe Length (100 m) Results. After the above model verification and parameter analysis, we extended the 10 m pipe to a 100 m length with the same settings as for the 10 m pipe. The 100 m pipe allows us to extend the time span in which the axial mixing occurs to 100 s (the superficial velocity that we kept at $u = 1$ m/s). With the longer pipe, entrance effects are certainly negligible.

The volume fraction profiles at different flow times (5, 10, 20, 40, 60, 80, and 100 s) are shown in Figure 4. The mixture length increases smoothly with the flow time increasing. After 100 s, the mixture length becomes as large as 2.14 m.

Figure 5 presents the detailed mixture length values according to the flow time from 5 to 100 s in the 100 m long pipe. On the basis of these results and eq 7, we can calculate an effective (cross-sectional-averaged) turbulent diffusivity as

$$\langle D_t \rangle = \frac{\delta^2}{\pi t} \tag{8}$$

where δ is the mixture length. This diffusivity is also shown in Figure 5. It shows that, after an initial decay, the diffusivity levels off to 0.0142 m^2/s; the 100 m pipe length suffices to confidently estimate the effective diffusivity in very long pipes.

On the basis of the above estimate for the effective diffusivity, we are now able to predict the mixture lengths after $t = 1000$ and 3000 s, corresponding to the mixing at the end of a 1 and 3 km pipe respectively: $\delta = (\langle D_t \rangle t)^{1/2}$. Inserting the values gives $\delta_{1000} = 6.76$ m and $\delta_{3000} = 11.7$ m. From a practical perspective, these numbers are used to set up the gas injection sequence to ignite the coal gasification process. The numbers also indicate that axial mixing has a limited extent and that the UCG system can work safely and reliably.

5. Further Calculation and Application

5.1. Effect of the Density Ratio. Thus far, we focused directly on an UCG application by considering mixing between fluids A and B. Here, we generalize by investigating the effect of the density ratio on the mixing process. If we designate the first injected liquid as fluid A and the second injected liquid as fluid B, we can define a density ratio as

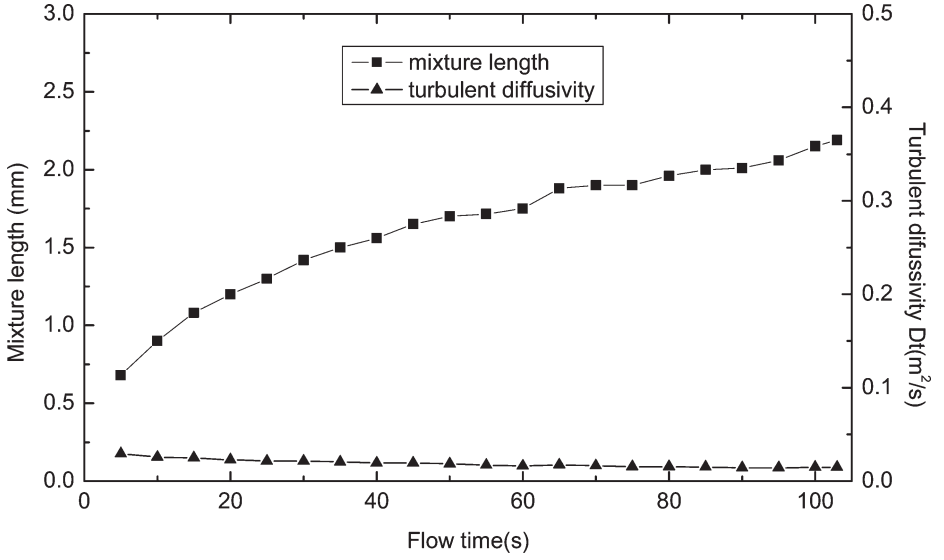

Figure 5. Mixture length and turbulent diffusivity in a 100 m horizontal pipe (diameter, 0.012 m; flow velocity, 1 m/s; *Re*, 20 000).

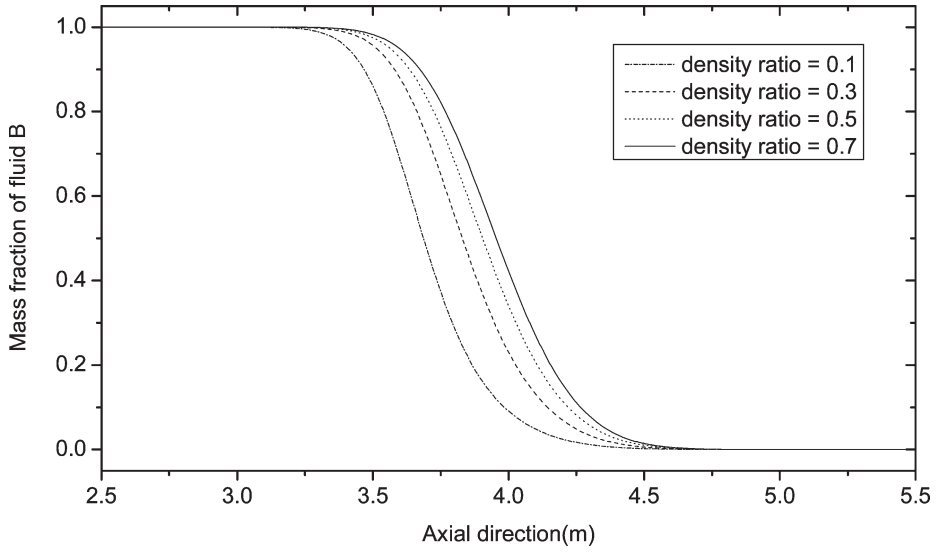

Figure 6. Mass fraction of fluid B at different density ratios (phase I is followed by phase II in the pipe).

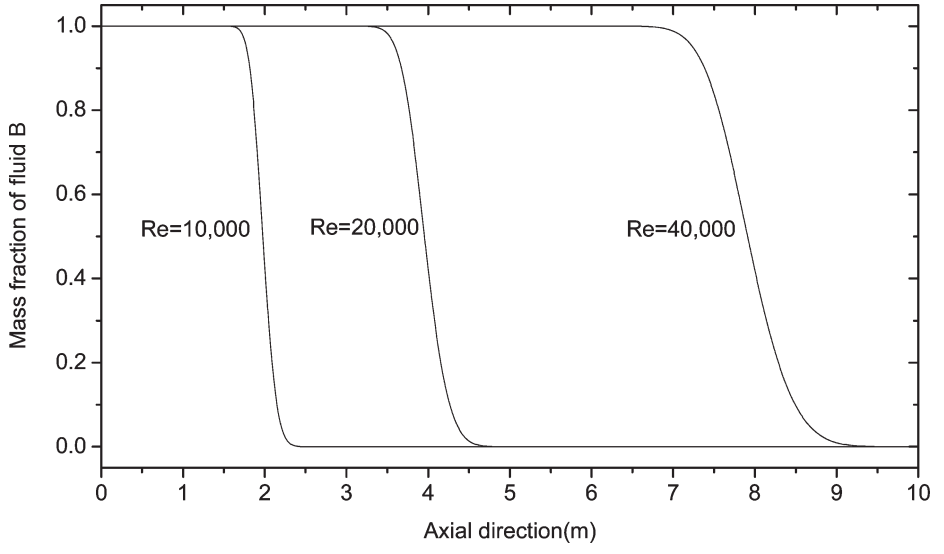

Figure 7. Mass fraction of fluid B at different *Re* numbers.

$r = \rho_{II}/\rho_I$. The density ratio of fluids A and B, r, for the base case is 0.7. We investigated mixing at $r = 0.1$, 0.3, and 0.5 as well. The results are listed in Table 1 and Figure 6. It is shown that a decrease of the density ratio gives a longer mixture length. The effect, however, is very weak, which could be anticipated because, as we saw above, buoyancy only weakly contributes to the axial mixing.

5.2. Reynolds Number Effects. The turbulence is the main driving force of mass-transfer and concentration diffusion in the turbulent flow. The volume fraction profile at different initial *Re* numbers (1.5×10^4, 3×10^4, and 6×10^4) when the other parameters are the same is shown in Table 1 and Figure 7. The mixture length is obviously becoming larger with the increase in the *Re* number. The increase of *Re* number contributes to the increase of turbulent parameters, such as k, ε, and turbulent viscosity, and give rise to the increase of species diffusion as a result. This means that, if we want to decrease the mixture effect in a horizontal pipe, we should decrease the *Re* number and turbulent level.

6. Conclusions

We performed time-dependent CFD simulations of the axial mixing of two different miscible liquids (different density and viscosity) in a long horizontal pipe, with turbulence and buoyancy as the main mixing mechanisms. The sensitivity of the results with respect to numerical parameters was first checked for a short (10 m) pipe. On the basis of this study, choices for time step and grid size in the axial direction were made. In the short pipe, we were also able to show that buoyancy is of a minor influence on axial mixing. Only if we increase the Richardson number to 10 times its actual value, buoyancy effects become significant.

A pipe length of 100 m proved sufficient to reliably estimate effective axial diffusivity, leading to predictions for the mixture lengths of 6.76 m after 1 km of pipe and 11.71 m after 3 km of pipe.

Because buoyancy has limited impact, the mixture length is not very sensitive to the density ratio of the two liquids involved. The impact of the Reynolds number on the mixture length is much larger, as could be anticipated because turbulence is the major driving force for axial mixing.

Acknowledgment. The authors acknowledge the financial support provided by the Alberta Energy Research Institute for this research.